AIMS Geosciences, 3 (2): 268-283
DOI: 10.3934/geosci.2017.2.268
Received date 14 February 2017
Accepted date 20 June 2017
Published date 29 June 2017

http://www.aimspress.com/journal/geosciences

Research article

Identifying Unlawful Constructions in Cultural Relic Sites Based on Subpixel Mapping—a Case Study in Mangshan Tombs, China

Yaping Xu [1], Lei Wang [1,*], Chengliang Liu [2] and Cuiling Liu [1]

[1] Department of Geography and Anthropology, Louisiana State University, Baton Rouge, LA 70803, USA

[2] School of Urban and Regional Science, East China Normal University, Shanghai 200062, China

* **Correspondence:** Email: leiwang@lsu.edu; Tel: +1-225-578-8876; Fax: +1-225-578-4420.

Abstract: Monitoring unlawful constructions in cultural relic sites is difficult in remote and unpopulated areas. This paper aims at facilitating cultural relic protection surveys using remote sensing. High-resolution remote sensing images are better alternatives to field visits for locating unlawful buildings. However, these buildings are usually hidden by vast wildness around the cultural relics, which makes the use of high-resolution imagery costly and inefficient. The main purpose of this research is to develop an approach to subpixel building identification from moderate resolution images, such as Landsat 8 OLI with reasonable accuracy based on the mixture-tuned match filtering (MTMF) partial unmixing method. With this method, pixels with high MF scores and low MT scores were identified as candidate locations of possible unlawful buildings. A case study in the Mangshan Tombs, China demonstrated that this method had a better accuracy for identifying constructions than the commonly used fully-constrained linear unmixing model.

Keywords: Cultural relic site protection; buildings identification; subpixel mapping; mixture-tuned match filtering (mtmf); Landsat

1. Introduction

To protect cultural relic sites, construction permits are required by law for new developments in relic sites and surrounding areas. However, the number of unpermitted buildings, mostly for private use, is still increasing [1]. This has made monitoring illegal constructions in cultural relic sites and world heritage sites an urgent task. These areas are mostly located in remote, mountainous, and unpopulated areas with limited accessibility. Due to this reason, frequent field visits to search for unlawful constructions are costly and sometimes impossible.

Modern geospatial technologies such as remote sensing (RS), geographic information system (GIS) and global positioning system (GPS) can fundamentally change the way to conduct cultural relic surveys [2,3]. For example, remote sensing images offer a synoptic view of the relic sites, thus making systematic and long term monitoring of land dynamics associated with human activities possible [2,3]. Although buildings are usually only visible from high-resolution commercial satellite images [2], such as the WorldView-3 satellites by DigitalGlobe, the use of moderate resolution images is still beneficial to the management agencies because they are less costly with much wider scene coverage. For example, the Landsat images, which are free to the public have a swath width of 180 km, ten times greater than WolrdView-3 images (13 km). In other words, one Landsat image is equivalent to over 100 WorldView-3 images in area coverage. However, previous research showed that such moderate resolution images did not provide accurate thematic classification maps by traditional classification algorithms [4,5] because the pixels are mostly mixtures of different lands. The mixed pixel problem becomes especially prevalent where the target buildings are small [6]. The low accuracy of building classification reflects the inability of traditional per-pixel classifiers to handle the mixed pixel problem [5].

Subpixel Mapping Analysis (SMA) is a solution to the mixed pixel problems. The SMA approach has proved reasonably accurate in climate change research [7–9], terrestrial ecosystem monitoring and management [10–12], precision agriculture and production monitoring [13–16], natural hazard risk assessment [17–19], forest inventories and forest health assessments [20–22], water quality assessment [23,24], geological mapping [25], mapping of the urban environment [26–30], urban land cover area [31,32] and more. A mixture model derives the fractions of a few “pure” materials in a mixed image pixel. These “pure” materials are usually called endmembers. Mixed pixel signals are generally modeled using either a linear mixture model (LMM) or nonlinear mixture model (NLMM). The linear unmixing model assumes the electromagnetic energy reflected from the earth's surface at different spectrums is the result of a linear combination of each of the endmembers [33]. Therefore, it is possible to use the least squares criterion to “unmix” these components to factions of pixel components [34–37]. But to do this one must assume to have full knowledge of materials in the scene [38]. This assumption, however, is quite difficult to fulfill given the complex land cover conditions in most applications, which makes the selection of endmembers a difficult yet critical step of spectral unmixing [39]. If by chance one of the materials is missing in the model, the solution to the

unmixing equations will be biased. If one wants to use multi-temporal images, the endmembers may vary on these images because of seasonal changes. Furthermore, some endmembers may only exist in certain images, which makes long-term monitoring more difficult.

Partial unmixing methods, such as the mixture-tuned match filtering (MTMF), relax the assumption of linear unmixing models by requiring only the knowledge about the target materials. It is thus more useful and feasible in the applications where only one material is concerned. MTMF has demonstrated superiority in geological mapping [40], vegetation classification [41,42]. But it has not been tested on mapping small buildings in an unpopulated area. The main objective of this research is to test if MTMF can outperform the fully constrained linear unmixing model. The knowledge gained from this research can guide the endeavors of using remote sensing in culture relic site protection.

2. Materials and Methods

2.1. Study sites and data

The study site falls within the Mangshan Tombs of Luoyang, Henan Province, China. Mangshan Tombs is one of China's largest national cultural relic protection units, composed of a large number of ancient burial sites, many of which are concentrated in certain areas. Mangshan Tombs range up to 746 square kilometers, extending into five counties and 46 villages. A total of 972 tombs have been found in Mangshan Tombs, including 24 imperial tombs, ranging from the Zhou Dynasty to the Qing Dynasty. For this reason, Mangshan Tombs is called “The Oriental Pyramid”. It is critically important to protect this relic site from unlawful construction activities, which could damage the ancient tombs [43]. The core protection area of Mangshan Tombs consists of three management zones: west, middle, and east. This research focuses on the western part (Figure 1).

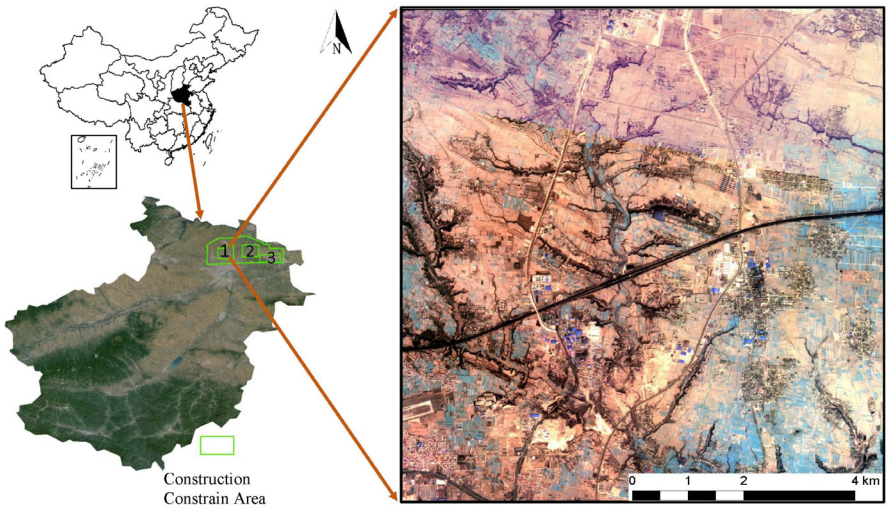

Figure 1. Location of Mangshan Tombs. (1.west part 2. middle part 3. east part).

Field investigation revealed there were mainly three types of buildings within the study area based on their roof colors: yellow, blue and red buildings (Figure 2). Yellow buildings are typically illegal temporary buildings for raising hogs or pigs, with minimum width or length between 5 and 20 meters. They are the primary purpose of our mapping effort. Blue buildings are typically for industrial purposes, with minimum width or length over 20 meters. They are mostly buildings with permits. However, as they could create harmful materials into the surrounding area, they will also be mapped. Red buildings are residential buildings with permits. They have the least impact on the relic tombs.

The images used in this research are listed in Table 1. We use the Landsat imagery to identify unlawful constructions within the study area, and the high-resolution Ziyuan-3 imagery for accuracy assessment. Table 2 lists the specifications of Ziyuan-3 data.

Table 1. Image data.

Data source	*Date*	*Level*	*Location*
Landsat 8	11/18/2013	l8_surface_reflectance	Mangshan Tombs
Ziyuan-3	03/20/2013	L1	Mangshan Tombs

Table 2. Ziyuan-3 specifications.

Bands	*Wavelength (micrometers)*	*Resolution (meters)*
Band 1-Panchromatic	0.45–0.80	2.1
Band 2-Blue	0.45–0.52	5.8
Band 3-Green	0.52–0.59	5.8
Band 4-Red	0.63–0.69	5.8
Band 5-Near Infrared (NIR)	0.77–0.89	5.8

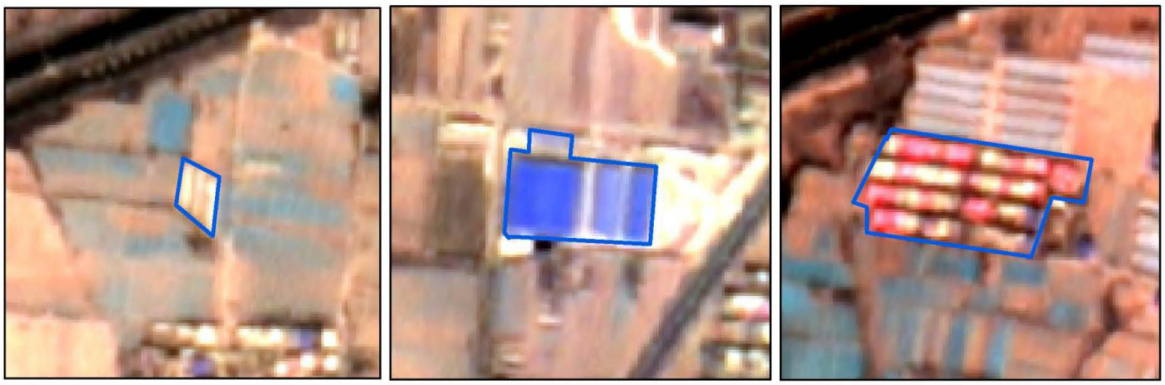

(a) (b) (c)

Figure 2. Building types in the study area (Ziyuan-3, RGB composition image). (a. yellow buildings; b. blue buildings; c. red buildings).

2.2. Mixture tuned matched Filtering

Matched filtering (MF) extracts the component of the material in an image pixel by comparing it to the target spectra and suppresses the response of all other unknown background spectra [44]. It distinguishes the target from the background but does not perform any further analysis on the content of the background materials. Thus, MF performs a partial unmixing of the spectra in each pixel of an image. MF requires only the target spectra, rather than a spectrum of all land cover materials in the scene. This is one of the major advantages of the MF algorithm. The mixture tuning (MT) filter was developed to address the cases where MF generates false positive results. The combined method is called mixture-tuned matched filtering (MTMF) [38]. MTMF combines the best features of the linear unmixing model and the statistical matched filter model while avoiding the drawbacks of the original methods [38], and is capable of detecting specific land cover types based on their spectral characteristics [45]. From matched filtering, it inherits the advantage of its ability to map a single known target without knowing the other background endmember signatures. From the linear unmixing model it inherits the constraints on feasibility including the unit-sum and positivity [38].

Matched filtering returns an MT score as the number of standard deviations from the mixing line which connects the background mean to the target spectrum. MT scores can be interpreted as unmixing infeasibility. High MT scores or infeasibility values, which mean a large separation from the signature of the target material, are used to identify false positives [38]. The methodology of this research consists of three major parts, data preprocessing, building identification from MTMF, and accuracy assessment and model comparison. Figure 3 shows the flowchart of the methodology.

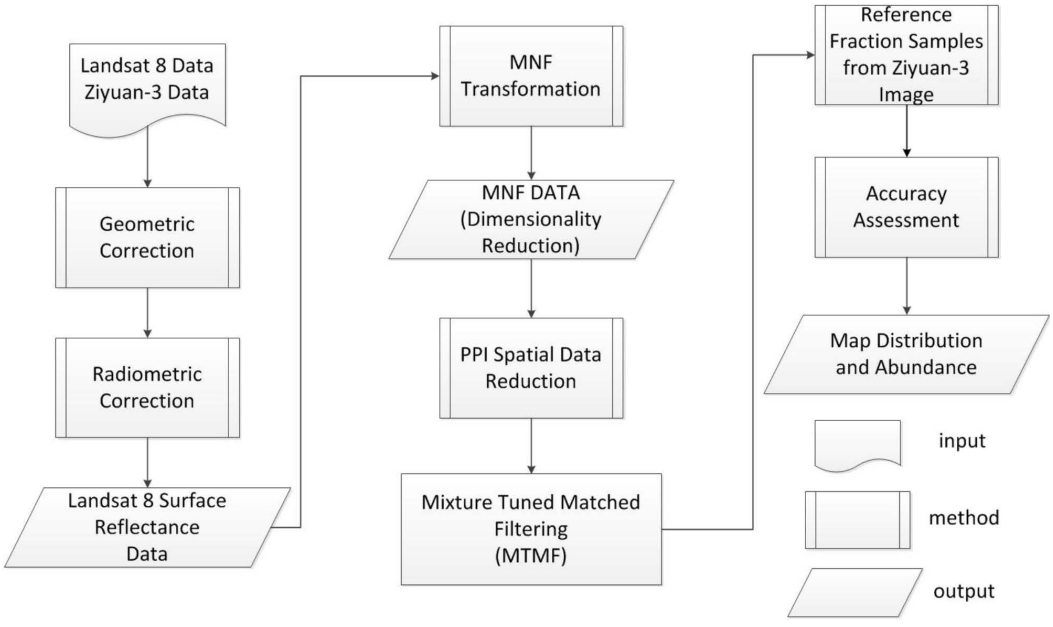

Figure 3. Research flowchart.

2.2.1. Data preprocessing

We used the Landsat Surface Reflectance product of the Landsat image produced by the United States Geological Survey with their atmospheric correction and radiometric calibration algorithm. Next, we applied a minimum noise fraction (MNF) method to the image to remove background noise prior to the MTMF algorithm [38,40,42,46].

The Ziyuan-3 image was used for accuracy assessment. We enhanced its multispectral resolution by fusing the high-resolution panchromatic band (2.1 m) into the multispectral bands. To adjust the alignment between the pixels from the Landsat image and the Ziyuan-3 image, we applied an image-to-image coregistration using an affine geometric transformation. Thirteen control points were identified from both images. The overall RMSE for the coregistration is 0.3941 image pixels.

2.2.2. Building identification from MTMF

Implementation of the MTMF algorithm included five steps: (1) remote sensing image atmospheric correction; (2) Minimum Noise Fraction (MNF) transformation; (3) pure pixels identification with Pixel Purity Index (PPI); (4) MF score and infeasibility output; and (5) target mapping from high MF scores. The ENVI Spectral Hourglass Wizard tool was used to aid the image analyses. Steps (1) and (2) were described in the last section. This section starts with step (3) to describe the procedure of the MTMF analysis.

Pixel Purity Index (PPI) calculates the possibility of an image pixel of being a pure pixel [47]. Pixels with higher PPIs are identified as candidates of pure pixels (often less than 1% of the total number of pixels). We used a threshold value of 2.5 times of the noise level (which is 1 for MNF transformed data) to identify these pure pixels (Figure 4).

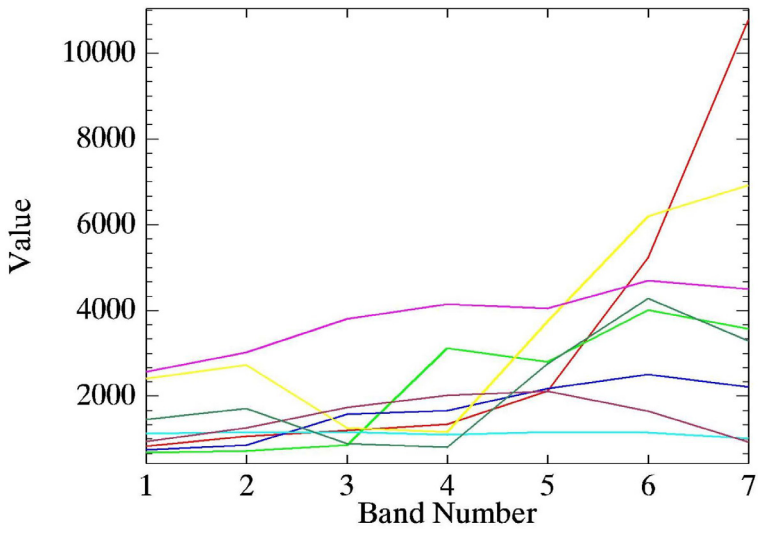

Figure 4. Spectra plot of endmembers (Landsat 8).

Figure 5 shows the MF score and infeasibility threshold determination through 2D scatter plot. A common way to find the thresholds is to interactively make selections on the scatter plot [38,41,42]. The scatterplot between MF scores and infeasibility values is used to filter out false positives. False positives are identified by their high infeasibility and low abundance (the pixels to the upper-left side of the threshold line). The valid pixels are to the lower-right side of the line. They will be used to map possible locations of illegal constructions. Higher MF scores mean there is high chance to find illegal buildings in those pixels [48].

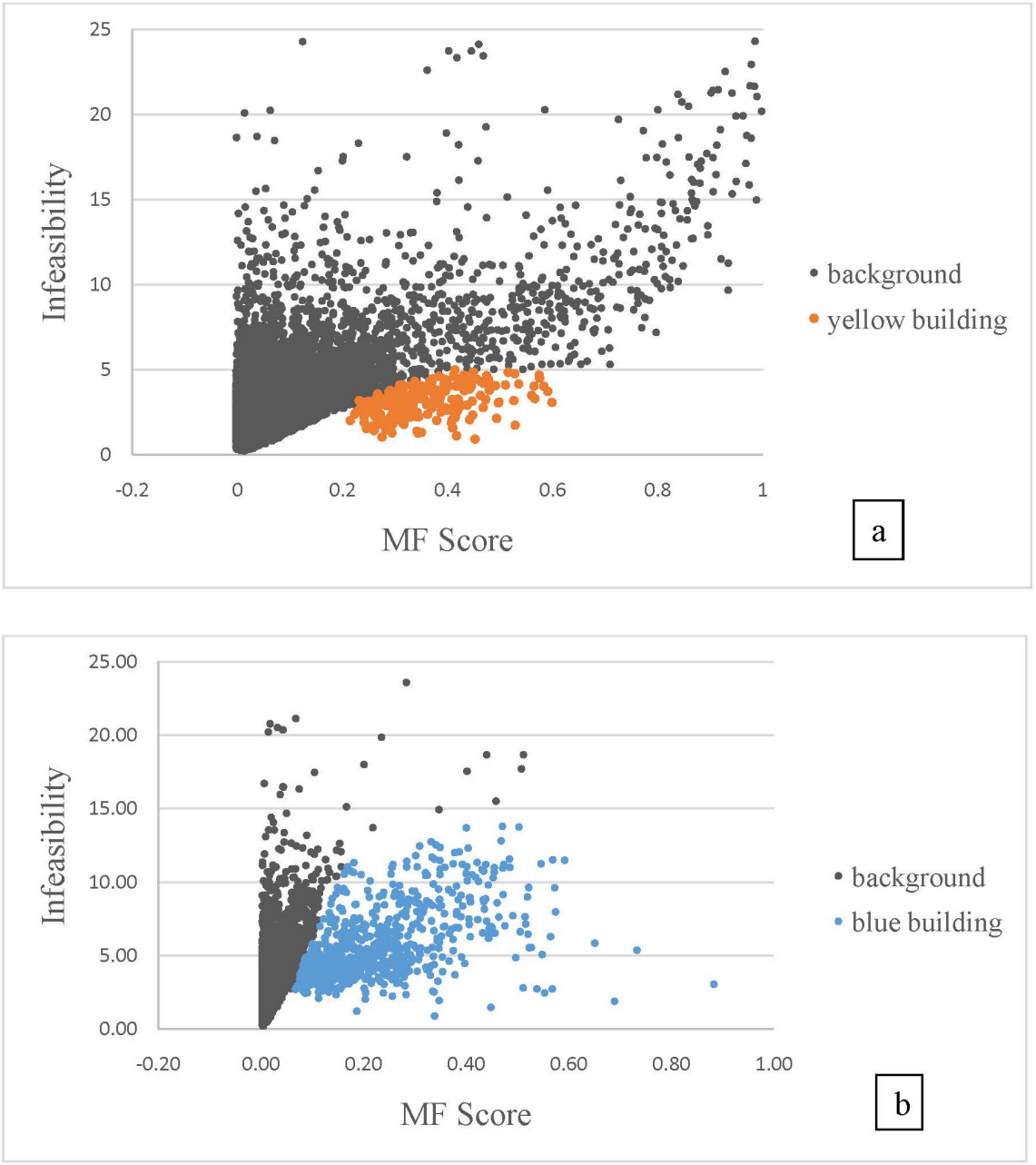

Figure 5. 2D scatter plot. The horizontal axis is the MF score (target abundance), the vertical axis is the MT score (infeasibility). (a. yellow building b. blue building).

2.2.3. Accuracy assessment and model comparison

We used a Ziyuan-3 high-resolution image to assess the accuracy of the MTMF results. The MTMF result is also compared to the output from a fully constrained linear unmixing analysis (LMA)[30]. We developed a two-step validation procedure. Step (1): for the full collection of reference sites, we applied confusion matrix and treated blue buildings and yellow buildings as two classes to examine their presence/absence [41,49–51]. Step (2), for sample targets, we used the correlation between reference fractions and modeled fractions to examine the accuracy [32,42]. We identified 27 random blue building samples and 29 yellow building samples as the targets. A quadrat sampling method [52] was then applied. The correlation between reference fractions and MF scores of building coverage was reported for each quadrat (30 m by 30 m Landsat pixel size). For convenience, the Ziyuan-3 image was resampled from 2.1 m by 2.1 m to 3 m by 3 m pixel size, which resulted in 100 Ziyuan-3 pixels in each Landsat pixel. An example of such quadrat sampling is shown in Figure 6. Within the Landsat pixel containing a yellow-roofed building, there are 24 of 100 Ziyuan-3 pixels belonging to the building. That is reported as a fraction value of 0.24 or 24%. An RMSE was then calculated based on the differences between the reference fraction and the MF scores from MTMF.

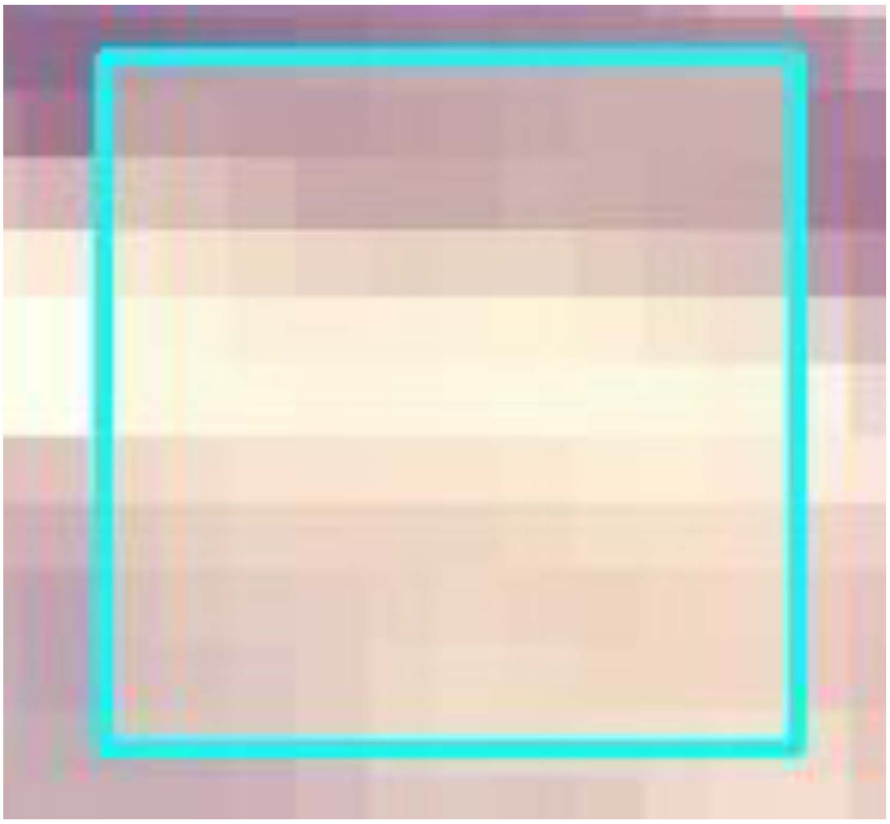

Figure 6. Application of quadrat sampling method (Ziyuan-3 image).

3. Results

The MTMF algorithm successfully identified both yellow and blue buildings. As shown in Figure 7 and Figure 8, both the yellow and blue buildings have strong signals from the MTMF method. In contrast, the LMA model produced a lot of false positives. For the MTMF method, both yellow and blue building classes yielded very high user accuracy. The MTMF method has a higher possibility to miss the yellow buildings than the blue buildings. It is expected because illegal buildings and some of the yellow buildings were constructed in small sizes. Blue buildings are generally industry buildings and are larger. As a result, mapping blue buildings is generally easier than mapping yellow buildings. Comparing to MTMF, the LMA method yielded lower accuracies (Table 3 and Table 4), both in the commission error (19.85%) and the omission error (58.85%).

Table 3. Accuracy assessment result of MTMF method.

Class	*Prod. Acc*	*User Acc*	*Commission*	*Omission*
	(Percent)	(Percent)	(Percent)	(Percent)
Yellow Building	51.15	95.34	4.66	48.85
Blue Building	70.72	99.61	0.39	29.28
Overall Accuracy = 59.18%				

Table 4. Accuracy assessment result of Linear Unmixing method.

Class	*Prod. Acc*	*User Acc*	*Commission*	*Omission*
	(Percent)	(Percent)	(Percent)	(Percent)
Yellow Building	41.15	80.15	19.85	58.85
Blue Building	62.98	99.56	0.44	37.02
Overall Accuracy = 50.11%				

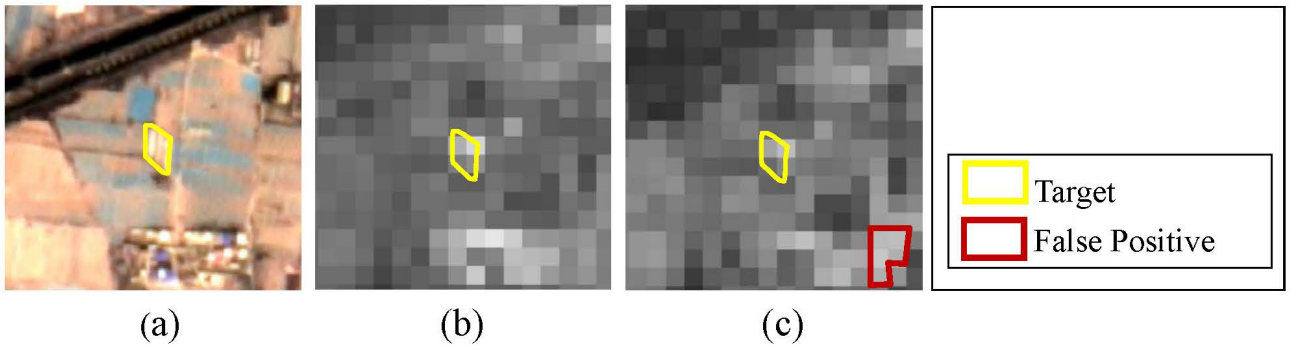

Figure 7. Yellow buildings identified from MTMF and Unmixing. (a. high-resolution image; b. yellow buildings identified from MTMF; c. yellow buildings identified from Unmixing).

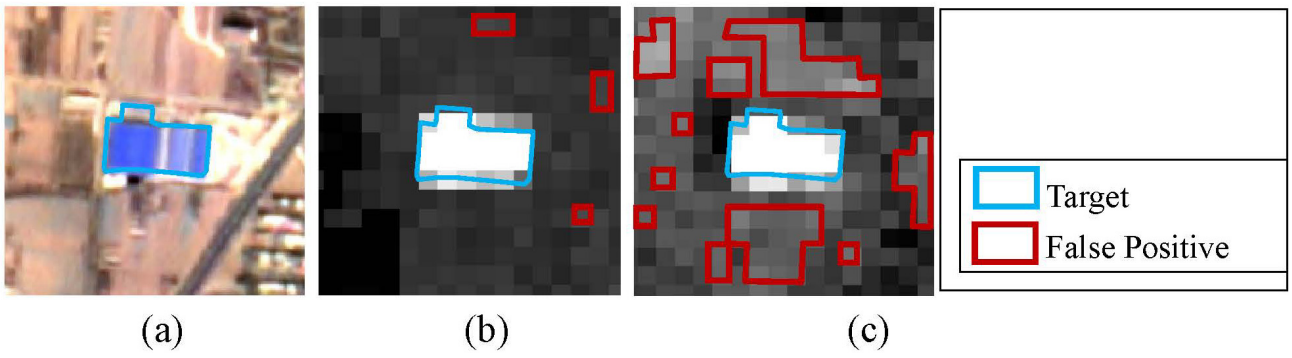

Figure 8. Blue buildings identified from MTMF and Unmixing. (a. high-resolution image; b. blue buildings identified from MTMF; c. blue buildings identified from Unmixing).

Our purpose is to identify suspicious areas with illegal buildings. Therefore, we would rather have lower omission errors on the yellow buildings by trading in high commission errors. One possible method to reduce omission errors is to make an adjustment on the MF score and infeasibility value through the 2D scatter plot. Figure 9 shows such a selection of MF score and infeasibility value to minimize the omission error (38.08%, Table 5).

The quadrat sampling method provided more assessments (Figure 10) than just commission errors and omission errors, which include the coefficient of determination (R^2), correlation coefficients, and RMSE, etc. For blue buildings, R^2 values were 0.81 (MTMF), 0.76 (LMA). For yellow buildings, the R^2 values were 0.75 (MTMF) and 0.60 (LMA). The correlation coefficients of MTMF results with the reference data were also much higher than that of the LMA results. The RMSEs were 0.146 (MTMF) and 0.160 (LMA) for yellow buildings (Table 6). The RMSEs for blue buildings are 0.143 (MTMF) and 0.157 (LMA). These RMSE values indicated that MTMF yielded a better result of mapping both yellow and blue buildings than the LMA method.

Table 5. MTMF accuracy based on optimized selection of MF score and infeasibility value.

Class	Prod.Acc (Percent)	User Acc (Percent)	Commission (Percent)	Omission (Percent)
Yellow Building	61.92	98.77	1.23	38.08
Blue Building	70.72	99.61	0.39	29.28
Overall Accuracy = 65.53%				

Table 6. RSME comparison between reference fractions and modeled fractions.

Methods	***MTMF***	***Linear Unmixing***
Yellow Buildings	0.146	0.160
Blue Buildings	0.143	0.157

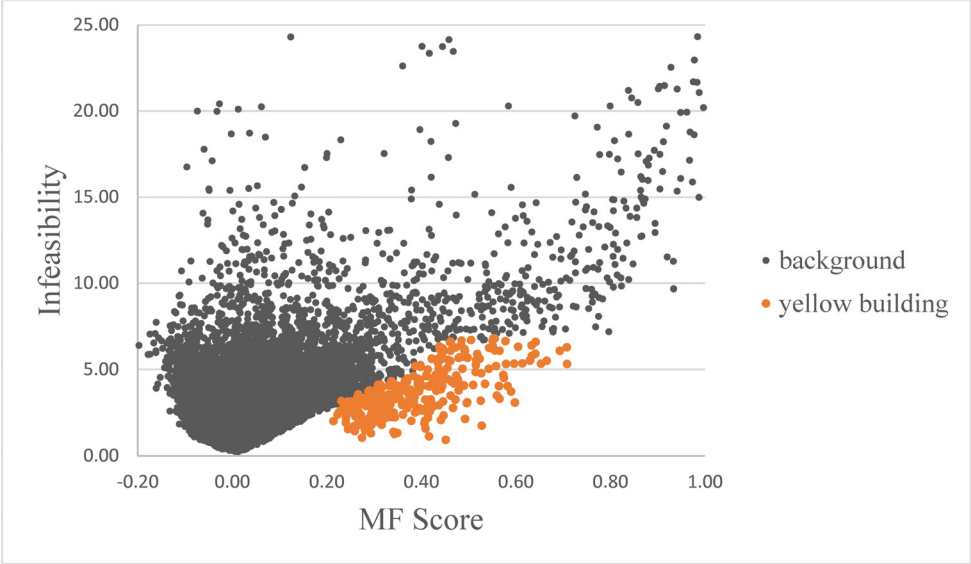

Figure 9. 2D scatter plot (X: MF Score; Y: infeasibility) for yellow buildings to reduce omission error.

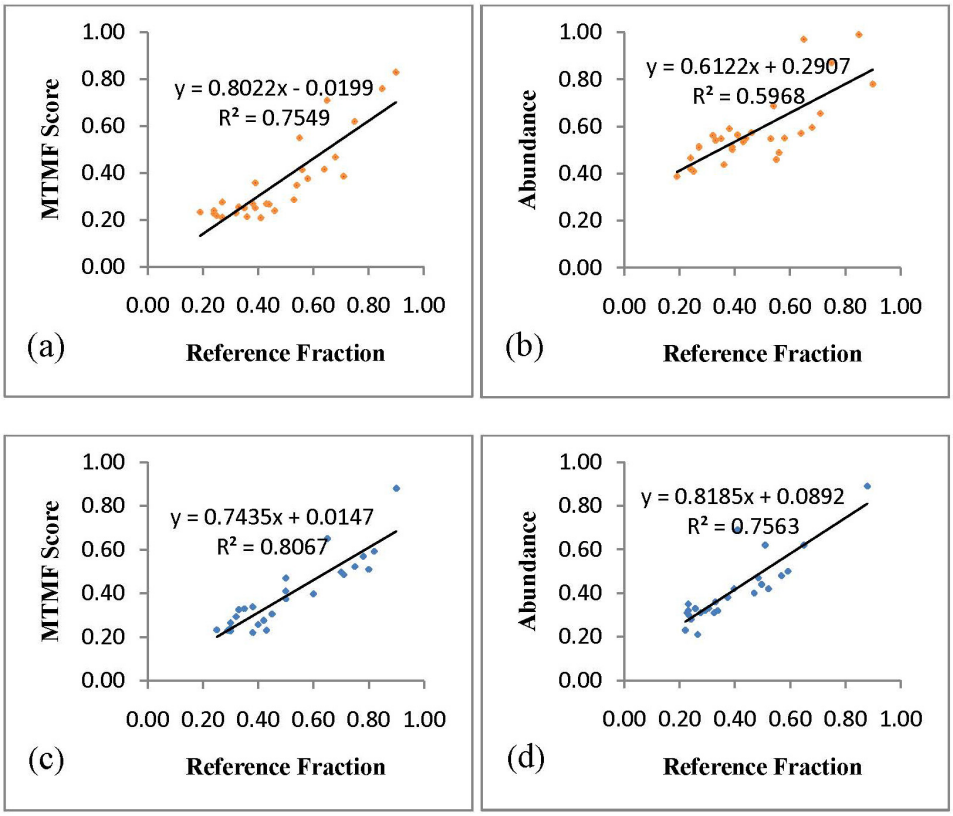

Figure 10. Regression between reference fractions and modeled fractions. (a & b yellow buildings; c & d blue buildings).

The illegal buildings are classified into the yellow roof buildings based on their intrinsic characteristics (yellowish roof, small, temporary, and built with less expensive materials). These illegal buildings will have moderate MF scores because they are generally much smaller than a 30 m by 30 m Landsat image pixel. Besides, the large and legal yellow buildings have larger MF scores. Therefore, the illegal buildings can be separated from those large yellow buildings. The identified illegal buildings are shown in Figure 11. Red colored areas are more likely to be an illegal building. Because our result contains large commission error, a field visit is still recommended for decision makers. But it has largely reduced the cost of field visits.

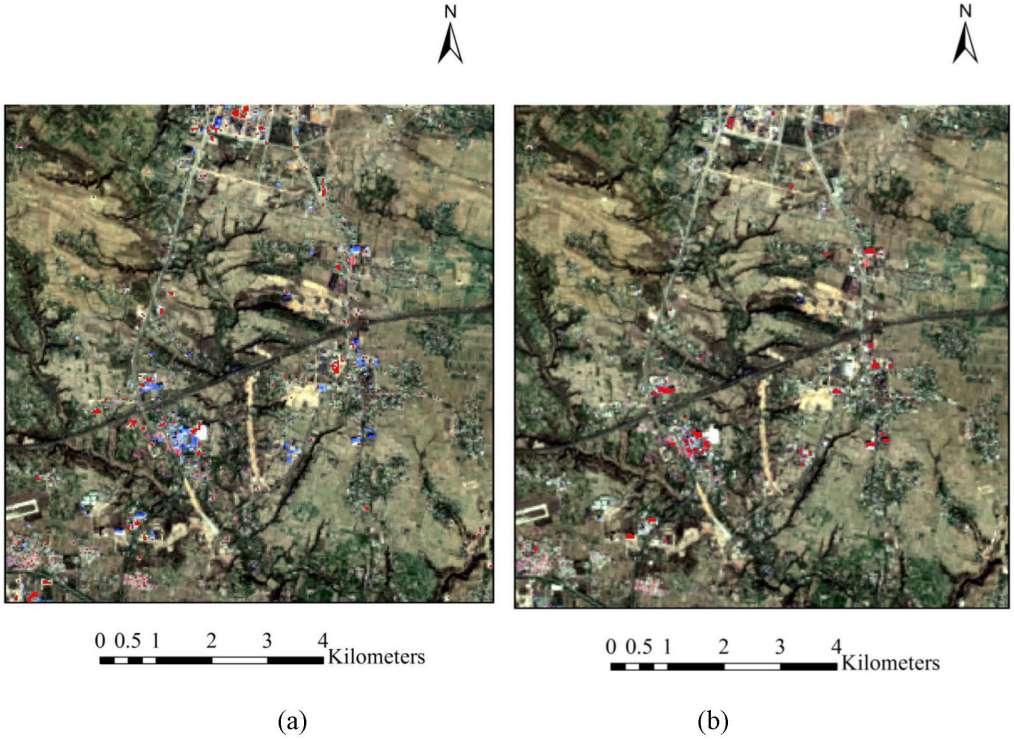

Figure 11. Buildings identification result. (a. yellow building b. blue building).

4. Summary and Conclusions

Cultural relic sites or heritage sites are often sparsely spread in large wildness; thus the illegal buildings in the relic are difficult to be identified unless high spatial resolution images are used. At the same time, high-resolution images come by high cost and small scene width. The main focus of this research is to develop an approach for building identification from moderate resolution images to lower the cost for searching the illegal constructions. We tested Landsat images with subpixel mapping methods to detect illegal buildings that are usually smaller than the image pixel size. We also compared the accuracy of the partial unmixing method Mixture-Tuned Matched Filtering (MTMF) with the fully constrained linear mixture analysis (LMA). Our results show that both unmixing methods could provide

reasonable accuracy of mapping the buildings (industry, illegal, and other buildings). Owing to the uncertainty from the subpixel analysis, mapping illegal buildings from satellites cannot fully replace ground surveys. However, our work could help expedite the ground survey process for illegal buildings by reducing the total area surveyed to a limited number of image pixels.

Our analysis confirmed that the partial unmixing method MTMF is stronger than the LMA method in mapping the buildings. Therefore, we recommend MTMF for long term illegal-building detection in relic sites. Besides, because MTMF only needs the information of the target spectra, it is extendable in both spatial and temporal domains.

Acknowledgments

This research was funded in part by a Robert C. West (or R.J. Russell) Graduate Student Field Research Award from the Department of Geography and Anthropology at Louisiana State University.

Conflict of Interest

All authors declare no conflicts of interest in this paper.

References

1. Morgan J (2010) Saving our vanishing heritage: safeguarding endangered cultural heritage sites in the developing world. Palo Alto: Global Heritage Fund, 37-42.
2. Lasaponara R, Masini N (2006) On the potential of QuickBird data for archaeological prospection. *Int J Remote Sens* 27: 3607-3614.
3. De Laet V, Paulissen E, Waelkens M (2007) Methods for the extraction of archaeological features from very high-resolution Ikonos-2 remote sensing imagery, Hisar (southwest Turkey). *J Archaeol Sci* 34: 830-841.
4. Malinverni ES, Fangi G (2009) Comparative cluster analysis to localize emergencies in archaeology. *J Cult Herit* 10: e10-e19.
5. Weng Q (2012) Remote sensing of impervious surfaces in the urban areas: Requirements, methods, and trends. *Remote Sens Environ* 117: 34-49.
6. Epsteln J, Payne K, Kramer E (2002) Techniques for mapping suburban sprawl. *Photogramm eng remote sens* 63: 913-918.
7. Asner GP, Heidebrecht KB (2005) Desertification alters regional ecosystem–climate interactions. *Glob Change Biol* 11:182-194.
8. Garcia M, Ustin SL (2001) Detection of interannual vegetation responses to climatic variability using AVIRIS data in a coastal savanna in California. *IEEE Trans Geosci Remote Sens* 39: 1480-1490.

9. Xu S, Peddle DR, Coburn CA, et al. (2008) Sensitivity of a carbon and productivity model to climatic, water, terrain, and biophysical parameters in a Rocky Mountain watershed. *Can J Remote Sens* 34: 245-258.
10. Gilabert MA, Garcıa-Haro FJ, Melia J. (2000) A mixture modeling approach to estimate vegetation parameters for heterogeneous canopies in remote sensing. *Remote Sens Environ* 72: 328-345.
11. Hestir Erin L, Khanna S, Andrew ME, et al. (2008) Identification of invasive vegetation using hyperspectral remote sensing in the California Delta ecosystem. *Remote Sens Environ* 112: 4034-4047.
12. Röder A, Udelhoven T, Hill J, et al. (2008) Trend analysis of Landsat-TM and-ETM+ imagery to monitor grazing impact in a rangeland ecosystem in Northern Greece. *Remote Sens Environ* 112: 2863-2875.
13. Lelong CC, Pinet PC, Poilvé H (1998) Hyperspectral imaging and stress mapping in agriculture: a case study on wheat in Beauce (France). *Remote sens environ* 66: 179-191.
14. Liu J, Miller JR, Haboudane D, et al. (2008) Crop fraction estimation from casi hyperspectral data using linear spectral unmixing and vegetation indices. *Can J Remote Sens* 34: S124-S138.
15. Lobell DB, Asner GP (2004) Cropland distributions from temporal unmixing of MODIS data. *Remote Sens Environ* 93: 412-422.
16. Pacheco A, McNairn H (2010) Evaluating multispectral remote sensing and spectral unmixing analysis for crop residue mapping. *Remote Sens Environ* 114: 2219-2228.
17. Eckmann TC, Still CJ, Roberts DA, et al. (2010) Variations in subpixel fire properties with season and land cover in Southern Africa. *Earth Interact* 14 : 1-29.
18. Jia GJ, Burke IC, Goetz AF, et al. (2006) Assessing spatial patterns of forest fuel using AVIRIS data. *Remote Sens Environ* 102: 318-327.
19. Katra I and Lancaster N (2008) Surface-sediment dynamics in a dust source from spaceborne multispectral thermal infrared data. *Remote sens Environ* 112: 3212-3221.
20. Goodwin N, Coops N C, Stone C (2005) Assessing plantation canopy condition from airborne imagery using spectral mixture analysis and fractional abundances. *Int J Appl Earth Obs Geoinform* 7: 11-28.
21. Peddle DR, Hall FG, LeDrew EF (1999) Spectral mixture analysis and geometric-optical reflectance modeling of boreal forest biophysical structure. *Remote Sens Environ* 67: 288-297.
22. Soenen SA, Peddle DR, Hall RJ, et al. (2010) Estimating aboveground forest biomass from canopy reflectance model inversion in mountainous terrain. *Remote Sens Environ* 114: 1325-1337.
23. Mertes LA, Smith MO, Adams JB (1993) Estimating suspended sediment concentrations in surface waters of the Amazon River wetlands from Landsat images. *Remote Sens Environ* 43: 281-301.
24. Svab E, Tyler AN, Preston T, et al. (2005) Characterizing the spectral reflectance of algae in lake waters with high suspended sediment concentrations. *Int J Remote Sens* 26: 919-928.
25. Bedini E (2009) Mapping lithology of the Sarfartoq carbonatite complex, southern West Greenland, using HyMap imaging spectrometer data. *Remote Sens Environ* 113: 1208-1219.

26. Phinn S, Stanford M, Scarth P, et al. (2002) Monitoring the composition of urban environments based on the vegetation-impervious surface-soil (VIS) model by subpixel analysis techniques. *Int J Remote Sens* 23: 4131-4153.
27. Rashed T, Weeks J R, Roberts D, et al. (2003) Measuring the physical composition of urban morphology using multiple endmember spectral mixture models. *Photogramm Eng Remote Sens* 69: 1011-1020.
28. Small C (2001) Estimation of urban vegetation abundance by spectral mixture analysis. *Int J remote sens* 22: 1305-1334.
29. Weng Q, Lu D, Schubring J (2004) Estimation of land surface temperature–vegetation abundance relationship for urban heat island studies. *Remote sens Environ* 89: 467-483.
30. Wu C, Murray AT (2003) Estimating impervious surface distribution by spectral mixture analysis. *Remote sens Environ* 84: 493-505.
31. Franke J, Roberts DA, Halligan K, et al. (2009) Hierarchical multiple endmember spectral mixture analysis (MESMA) of hyperspectral imagery for urban environments. *Remote Sens Environ* 113: 1712-1723.
32. Powell RL, Roberts DA, Dennison PE, et al. (2007) Sub-pixel mapping of urban land cover using multiple endmember spectral mixture analysis: Manaus, Brazil. *Remote Sens Environ* 106: 253-267.
33. Adams JB, Sabol DE, Kapos V, et al. (1995) Classification of multispectral images based on fractions of endmembers: Application to land-cover change in the Brazilian Amazon. *Remote Sens Environ* 52: 137-154.
34. Atkinson PM, Cutler ME, LewisH (1997) Mapping sub-pixel proportional land cover with AVHRR imagery. *Int J Remote Sens* 18: 917-935.
35. Atkinson PM (2009) Issues of uncertainty in super-resolution mapping and their implications for the design of an inter-comparison study. *Int J Remote Sens* 30: 5293-5308.
36. Foody GM (2002) The role of soft classification techniques in the refinement of estimates of ground control point location. *Photogramm Eng Remote Sens* 68: 897-904.
37. Mertens KC, Verbeke LPC, Ducheyne EI, et al. (2003) Using genetic algorithms in sub-pixel mapping. *Int J Remote Sens* 24: 4241-4247.
38. Boardman JW, Kruse FA (2011) Analysis of Imaging Spectrometer Data Using-Dimensional Geometry and a Mixture-Tuned Matched Filtering Approach. *IEEE Trans Geosci Remote Sens* 49: 4138-4152
39. Plaza A, Martínez P, Pérez R, et al. (2004) A quantitative and comparative analysis of endmember extraction algorithms from hyperspectral data. *IEEE trans geosci remote sens* 42: 650-663.
40. Goodarzi Mehr S, Ahadnejad V, Abbaspour RA, et al. (2013) Using the mixture-tuned matched filtering method for lithological mapping with Landsat TM5 images. *Int J Remote Sens* 34: 8803-8816.
41. Mundt JT, Streutker DR, Glenn NaF (2007) Partial unmixing of hyperspectral imagery: theory and methods. *Proc Am Soc Photogramm Remote Sens*.

42. Mitchell JJ, Glenn NF (2009) Subpixel abundance estimates in mixture-tuned matched filtering classifications of leafy spurge (Euphorbia esula L.). *Int J Remote Sens* 30: 6099-6119.
43. Chen G, Zheng Z, "The Oriental Pyramid" Mangshan Tombs now total 972 mass graves. China News, 2009. Available from: http://www.chinanews.com/cul/news/2009/09-22/1879934.shtml.
44. Harsanyi JC, Chang CI (1994) Hyperspectral image classification and dimensionality reduction: an orthogonal subspace projection approach. *IEEE Trans geosci remote sens* 32: 779-785.
45. Harris A, Bryant RG (2009) A multi-scale remote sensing approach for monitoring northern peatland hydrology: Present possibilities and future challenges. *J environ manag* 90: 2178-2188.
46. Brelsford C, Shepherd D (2014) Using mixture-tuned match filtering to measure changes in subpixel vegetation area in Las Vegas, Nevada. *J Appl Remote Sens* 8: 083660-083660.
47. Boardman JW, Kruse F A, Green RO (1995) Mapping target signatures via partial unmixing of AVIRIS data.
48. Harris, Mixture Tuned Matched Filtering. Harris Geospatial Solutions,2016. Available from: https://www.harrisgeospatial.com/docs/mtmf.html.
49. Lu D, Weng Q (2004) Spectral mixture analysis of the urban landscape in Indianapolis with Landsat ETM+ imagery. *Photogramm Eng Remote Sens* 70: 1053-1062.
50. Parker AE, Hunt ER (2004) Accuracy assessment for detection of leafy spurge with hyperspectral imagery. *J Range Manag* 57: 106-112.
51. Mundt JT, Glenn NF, Weber K T, et al. (2005) Discrimination of hoary cress and determination of its detection limits via hyperspectral image processing and accuracy assessment techniques. *Remote Sens Environ* 96: 509-517.
52. Snyder RA, Boss CL (2002) Recovery and stability in barrier island plant communities. *J Coast Res* 18: 530-536.

AIMS Press